Numerical simulation of thin-shell direct drive DHe3-filled capsules fielded at OMEGA

A. R. Miles, H.-K. Chung, R. Heeter, W. Hsing, J. A. Koch et al.

Citation: Phys. Plasmas **19**, 072702 (2012); doi: 10.1063/1.4737052
View online: http://dx.doi.org/10.1063/1.4737052
View Table of Contents: http://pop.aip.org/resource/1/PHPAEN/v19/i7
Published by the American Institute of Physics.

Numerical simulation of thin-shell direct drive DHe3-filled capsules fielded at OMEGA

A. R. Miles,[1] H.-K. Chung,[1] R. Heeter,[1] W. Hsing,[1] J. A. Koch,[1] H.-S. Park,[1] H. F. Robey,[1] H. A. Scott,[1] R. Tommasini,[1] J. Frenje,[2] C. K. Li,[2] R. Petrasso,[2] V. Glebov,[3] and R. W. Lee[4]
[1]*Lawrence Livermore National Laboratory, Livermore, California 94550, USA*
[2]*Plasma Science and Fusion Center, Massachusetts Institute of Technology, Cambridge, Massachusetts 02139, USA*
[3]*Laboratory for Laser Energetics, University of Rochester, Rochester, New York 14623, USA*
[4]*SLAC Linear Coherent Light Source, Menlo Park, California 94025, USA*

(Received 12 April 2012; accepted 11 June 2012; published online 17 July 2012)

Thin-shell deuterium-helium-3 (DHe^3) filled glass capsules on the Omega laser provide a fast-implosion experimental platform for developing separate time-resolved measurements of ion, electron, and radiation temperatures in nonequilibrium plasmas. Dynamically significant non-local thermodynamic equilibrium (NLTE) conditions are created by the addition of xenon dopant to the DHe^3 gas fill, in quantities sufficient to have an impact on yields, compression, and cooling rates. The high-Z dopant dramatically increases the radiative cooling rate in the plasma, allowing it to collapse in compressions that can be an order of magnitude higher than in undoped capsules. A baseline LASNEX simulation model using detailed configuration accounting NLTE atomic physics shows very good agreement with the data for doped as well as undoped capsules, while other models either underpredict or overpredict the radiative cooling enhancement. The baseline model captures the behavior of the capsule when the D:He^3 ratio is varied well away from equimolar, suggesting no yield anomaly with either nearly pure deuterium or He^3 fills. Variation of the electron-ion coupling in the baseline simulation model shows agreement with the data for a coupling multiplier that is within 20% of unity. Reliably inferring electron-ion coupling strength from the data is complicated by uncertainties in the hydrodynamic mix and other parameters, but many of these can be mitigated in follow-on experiments at the National Ignition Facility. [http://dx.doi.org/10.1063/1.4737052]

I. INTRODUCTION

Laser-drive capsule implosions can be used to access high-energy-density (HED) plasma conditions for inertial confinement fusion (ICF). Rapid plasma heating, whether by strong shocks or alpha particle energy deposition, can drive the plasma out of thermal equilibrium.[1,2] Because ion-electron equilibration times are much longer than ion-ion or electron-electron collision times, each plasma species can in many cases be described by a Maxwell-Boltzmann distribution with associated temperature even when those temperatures are not equal for all plasma species. For example, a strong shock will preferentially heat ions, and the resulting ion-electron temperature differential might persist over dynamically significant timescales. Similarly, the radiation field might be coupled to the matter sufficiently weakly that the effective radiation temperature, $Tr = (E_r/a)^4$ (where E_r is the radiation energy density), remains well below any matter temperature. Energy coupling in such nonequilibrium plasmas is governed by interparticle interactions and radiative processes, which all work to drive the plasma back towards thermal equilibrium at a single temperature.

These couplings are further complicated when higher-Z plasma species are added to the mix, either due to hydrodynamic instabilities or intentionally as a spectroscopic temperature diagnostic. When plasma temperatures are high and the density is low, recombination and line radiation from partially ionized high-Z dopants can escape the plasma, and atomic populations are determined by radiative rates as well as collisional rates at the local plasma and temperature. This condition is known as nonlocal thermodynamic equilibrium (NLTE).[3] The absence of local thermodynamic equilibrium (LTE) significantly complicates the task of numerically modeling the plasma, as an accurate description then depends on detailed atomic physics modeling. In NLTE, atomic level populations are determined by radiative as well as collisional processes, and must be calculated by solving the photon-distribution-dependent rate equations. The equation of state (EOS), opacity, and ionization states are then determined from the atomic populations.

Note that LTE does not imply thermal equilibrium. That is, ion and electron temperatures can be unequal (plasma out of temperature equilibrium) while the individual temperatures as well as the EOS, opacity, and ionization states are still determined by collisional processes at the local fluid temperature and density (plasma in LTE).

Different NLTE models include varying degrees of sophistication and detail, and can give very different atomic populations under given plasma conditions. The more sophisticated models can be very computationally expensive, so it is not always practical to run what is believed to be the best model. Because of the uncertainties associated with these models, it is very important to have experiments with

observables that are sensitive to differences in NLTE modeling.

At the OMEGA (Ref. 4) laser facility at the University of Rochester's Laboratory for Laser Energetics, we have fielded thin glass shells filled with deuterium-helium-3 (DHe^3) thermonuclear (TN) fuel. The thin shell results in a fast implosion behind a strong shock. The shock drives the plasma out of equilibrium during the implosion, with $T_i > T_e > T_r$, and this condition persists until well after bounce (i.e., minimum volume) and into the subsequent re-expansion. Peak ion temperatures are ~7–10 keV in undoped capsules, and peak electron temperatures are ~3 keV. The ultimate goal of this effort is to develop an ICF platform that provides separate, time-resolved measurements of T_i, T_e, and T_r, in a nonequilibrium plasma that can be brought into a state of NLTE via the addition of small amounts of high-Z gas dopants to the fuel. The resulting NLTE effects can have a significant impact on the capsule implosion dynamics.

II. EXPERIMENT DESCRIPTION

The SiO_2 capsules used in this study have a nominal outer diameter of about 900 μm (870 ± 30 μm) and a wall thickness of about 4 μm (3.9 ± 0.2 μm), and were fabricated by General Atomics.[5] The nominal gas fill is 10 atm of deuterium and helium-3. The nominal partial pressures are 6.67 atm of D_2 and 3.33 atm of He^3, corresponding to atomic fractions of 0.8 for D and 0.2 for He^3. This ratio was chosen to be near the optimum for DHe^3 proton yield.

In addition to the low-Z thermonuclear fuel, the capsules contain up to three types of higher-Z material. First of all, varying amounts of xenon dopant is added to the gas (in the range of 0.1–0.7 at. %) in about half of the capsules in order to affect the ion-electron and matter-radiation couplings, and to introduce dynamically significant NLTE effects. Smaller amounts of krypton (in the range of 0.05%–0.5%) are typically also added as a spectroscopic electron temperature diagnostic. The Kr dopant levels are limited such that they are not dynamically significant. That is, the Kr does not affect the yields, temperatures, convergence ratio (CR), etc. This limit is set by LTE computer simulations (which are conservative in that they overestimate radiative losses due to high-Z dopants) and is verified experimentally. Finally, the glass shell fabrication process results in small amounts of residual gases, the dominant component of which is up to about 0.5 atm of CO_2.

The capsules are driven with all 60 Omega laser beams. The nominal pulse duration is 800 ps, (with 100 ps rise and fall). The nominal laser energy is ~18 kJ, with individual pulses in the range of about 16–18 kJ. The resulting laser intensity at the capsule surface ranged from about (0.5–1.0) $\times 10^{15}$ W/cm^2. Typical DD neutron yields for these capsules are of order 10^{11}, while DHe^3 proton yields are of order 10^{10}.

The experimental campaign consisted of seven shot weeks: two per year from late 2005 through 2008. Each shot week included several individual capsule implosions, ranging from 4 to 12 shots per week. Because the overall campaign included significant deviations from the nominal capsule parameters described above, it is worth briefly summarizing each one.

Series 0 (6 shots in November, 2005) lead off the campaign with a longer, higher-energy laser pulse (~23 kJ in 1 ns) than that described above. In these first experiments, it was found that the bang time (the time of peak reaction rate) occurred before the end of the laser pulse, prompting concern that hot electron production might affect diagnostics around this time.

This was mitigated in series 1 (7 shots in March, 2006) by reducing the laser pulse duration to 800 ps. Since the nominal laser power was not decreased, this results in a reduction in nominal laser energy from 23 kJ down to the 18 kJ reported above. An alternative approach was tested in series 2 (6 shots in August, 2006), in which the longer pulse was retained but the capsule diameter was increased to ~1100 μm, which brought with it a larger average shell thickness of about 5 μm. The thicker shells gave lower burn temperatures, which would make spectroscopic electron temperature measurements more difficult, and there was concern that the larger diameter would result in greater laser nonuniformity on the capsule surface.

Consequently, we returned to the smaller capsule (900 μm diameter) and shorter laser pulse duration (800 ps) for all subsequent shots. series 3 and 4 (4 shots in June, 2007 and 12 shots in August, 2007) included 9 shots with Xe dopant and 6 undoped capsules. In the final two series, we varied the ratio of He^3 to D in response to anomalous yield observations reported by others in similar experiments. In addition to off-nominal He^3 ratios, series 5 (5 shots in March, 2008) and series 6 (6 shots in December, 2008) included three nominal-fill undoped target and 1 nominal-fill doped target.

III. DIAGNOSTICS

A broad suite of diagnostics was used to characterize the capsule implosion. Neutron temporal diagnostic (NTD)[6] and proton temporal diagnostic (PTD)[6–8] give neutron and proton production rates vs. time, as well as total particle yields. Neutron time of flight (nTOF) diagnostic[9] gives DD and DT neutron yields, as well as DD burn-weighted ion temperature via thermal Doppler broadening of the arrival pulse. There is no tritium included in the capsule gas fill, so all DT neutrons are due to in-flight reactions between tritons produced in DD reactions, and background deuterium ions. Consequently, the ratio of secondary DT neutrons to primary DD neutrons gives a measure of the DD burn-weighted ρR of the fuel, or capsule compression.[10–14]

Wedge range filters (WRFs) give proton spectrum as well as a second measure of DHe^3 proton yield.[15] The downshift in DHe^3 proton energies gives a measure of the DHe^3 burn-weighted ρR of the gas plus shell.[15]

TN reaction weighted temperatures are inferred from the parabolic profile model (PPM) method developed by Frenje *et al.*[16] This method uses DD neutron and DHe^3 proton rate histories, together with model radial profiles of density and temperature, and was applied to only a few of the capsules in this study.

Electron temperatures are inferred from bremmstrahlung continuum and, where possible, Kr K-shell line emission. A Livermore-developed streaked conical mica crystal spectrometer[17] was used to measure time-resolved x-ray spectra, and a High-Energy Electronic X-ray (HENEX) spectrometer[18] developed by the Naval Research Laboratory and National Institute for Standards and Technology was used for high-quality time-integrated spectra. Gated framing cameras are used to image the size and shape of the hot x-ray emitting core.

In this paper, we focus on thermonuclear yields, fuel compression via the DT/DD neutron ratio, and time-integrated burn-weighted temperatures. Spectroscopic diagnostics will be discussed in a later publication.

IV. COMPUTER SIMULATIONS

The experiments are modeled in 1D using the radiation hydrodynamics code LASNEX.[19] Due to variations in capsule dimensions, fill, and laser drive, each experiment is modeled individually. The simulations include multigroup flux-limited radiation diffusion, electron and ion thermal conduction, Spitzer-Braginskii plasma viscosity, thermonuclear burn, and charged particle transport. Equations of state and multigroup opacities can either be tabular (if LTE), or else supplied by the atomic physics model.

The laser package does 3D laser raytrace with the specified beam spatial profile (order 4.1 superguassian with radius of 360 μm), assuming that the 1D rad-hydro simulation represents a spherically symmetric target. Laser energy deposition is via inverse bremmstrahlung. Because there is no accounting for laser-plasma interactions and kinetic effects in the absorption region, we reduce the incident laser energy by a factor *lasfac*, which is adjusted in concert with the electron thermal conduction flux limiter[20] based on the implosion timing data. For the results presented here, we use $lasfac = 0.70$ and a flux limiter f_e of 0.071.

The amount of CO_2 contaminant in the gas is not known precisely for each capsule, but is estimated to be in the range of 0.1–0.5 atm. For the calculations reported here, we fix the CO_2 level at the maximum 0.5 atm. The reasoning for this choice, as well as the sensitivity of the calculations to the CO_2 pressure, are discussed in Sec. VI B below.

Various options are available for handling the atomic physics. The first approach uses LTE tabular opacities and equations of state, and will be referred to simply as LTE. The XSNQ model is the NLTE version of the XSN atomic physics model.[21] XSN is an average atom atomic physics code based on a Z-scaled screened hydrogenic model, which performs in-line calculations to provide EOS and opacity for arbitrary mixtures at specified temperature and density. XSNQ solves rate equations for a single (average) ionization state to obtain the EOS and opacities. The model's lack of detail and its approximate treatment of bound states severely limits the accuracy of its spectral opacities. Despite these shortcomings, its frequency-averaged opacities are often surprisingly good. XSNQ is best used for when spectral details are unimportant, e.g., optically thick plasmas.

The more sophisticated detailed configuration accounting (DCA) model solves the rate equations for the number of ions in each important level in each ionization state, for each element.[22] It can handle any number of states connected by radiative and collisional bound-bound, bound-free, autoionization, and dielectronic recombination processes. The states and transition rates can be specified in data files generated by other codes, or via a simple screened hydrogenic model. To date, we have only used the latter option (screened hydrogenic) in modeling these experiments with DCA. The DCA model can also include line transfer effects with a general-purpose escape probability method. DCA is expected to be more appropriate than XSN when more detailed atomic physics is needed. This is the case for our Xe dopant, which is ionized to the L-shell and includes important optically thin transitions. Indeed, we find that DCA agrees with the data much better than either LTE or XSNQ. Thus, all results reported here use the DCA model, except where we explicitly discuss sensitivity to atomic physics modeling.

When using an NLTE model, LASNEX offer different options for treating energy-temperature consistency. In the default energy mode (which we will call DCA:E), the code insists on energy-temperature consistency with energy conservation. To do this, the energy and temperature are obtained from the radiation transport equation, which conserves energy and assumes a fixed specific heat in each zone to calculate temperatures. This solution method does not ensure that the two satisfy the EOS at the current density. The temperature is then reset with a call to the EOS at the calculated (conserved) energy, using the specific heat. For LTE zones, material energy density depends only on the temperature (for fixed density) as described by the specific heat. The non-linearity of this dependence usually results in very small corrections to the temperatures. For NLTE zones, the material energy density also depends on the radiation field. The specific heats are calculated assuming a fixed radiation field (from the previous time step) and do not describe the dependence on the radiation field, even if the radiation is Planckian. In this case, the temperatures corrections required to conserve energy can be more substantial.

Under the alternative temperature mode option (which we call DCA:T), the electron and ion energies are instead recalculated from their temperatures. This might be a better approximation for low-density NLTE material where the EOS is more sensitive to temperature than it is to energy. In our Omega experiments, we find slightly better overall agreement with DCA:E, and so it is used for our baseline.

V. SIMULATION STRATEGY

Before comparing simulations with the data, we first summarize our approach to setting the adjustable parameters available in the code to match the data. Because we anticipate sensitivity to NLTE atomic physics modeling, our general strategy is to set all other parameters based solely on the data from capsules without Xe dopant.

We first scale the incident laser energy down by a factor $lasfac = 0.70$ in order to account for energy loss to laser-plasma interactions and kinetic effects such as hot electron production, and use an electron flux limiter $f_e = 0.071$. These

values are chosen to match on average the observed implosion timing data from the 14 nominal-fill undoped capsules in series 1, 3, 4, 5, and 6 (nominal capsule and gas fill). We acknowledge, however, that this choice is not unique. That is, we could match the timing data equally well by reducing *lasfac* and increasing the flux limiter to compensate for lower incident laser energy. For example, we find equally good agreement with timing data at the values $lasfac = 0.63$ and electron flux limiter $f_e = 0.145$, which were arrived at by Dodd *et al.*[23] based on measurements of backscattered laser light in experiments[24,25] with capsules very similar to ours. Their slightly larger diameter ($\sim 925\,\mu$m) and thickness ($\sim 5.0\,\mu$m) capsules were driven by the longer 23 kJ pulse used in our shot series 0 and series 2. Longer drive pulse duration relative to implosion time might give lower efficiency energy coupling, however, our baseline model calculations do not appear to be energy rich compared to our limited series 0 data, which used the 1 ns drive pulse. Finally, we note that in the limiting case that we do not dial down the incident laser energy ($lasfac = 1.0$), we need an electron flux limiter $f_e = 0.051$.

The second step is to adjust the mix model to give a reasonable match, on average, to both the neutron and proton yields. Finally, the unknown CO_2 concentration is allowed to vary between 0.1 and 0.5 atm. This has some effect on the yields and burn temperatures, but neither mix nor CO_2 pressure (within this range) has a large impact on the implosion timing. The process of adjusting mix and CO_2 concentration is iterated until reasonable average agreement is found with all the undoped nominal capsules. These values are then fixed for all capsules, including the 13 shots with Xe, so that we are running a common model.

The simulations include three material regions: the glass shell, the gas within it, and a low-density helium atmosphere surrounding the capsule. Tabular EOS and opacities are used for the shell, the atmosphere, and the gas in cases where Xe and Kr are not present. When the Xe and/or Kr pressures are set to greater than zero, NLTE physics is triggered in the gas region only, with the DCA:E model used as the baseline.

VI. COMPARISON OF SIMULATION RESULTS WITH EXPERIMENT

A. Average level of agreement

Figure 1 shows the average relative deviation between the baseline simulations and the data for undoped capsules (Fig. 1(a)) and doped capsules (Fig. 1(b)). In these plots, the error bars denote the standard deviation in the agreement, and the solid lines show the experimental uncertainty in a single measurement of that quantity.

Experimental nTOF ion temperatures are compared with simulated ion temperatures derived from the width of the DD neutron creation spectrum. The simulation value accounts for thermal and bulk velocity Doppler broadening, but does not account for broadening due to finite burn time or finite fuel region crossing time. However, we have estimated for these effects a less than 0.1% contribution to the burn temperature inferred from the nTOF signal.

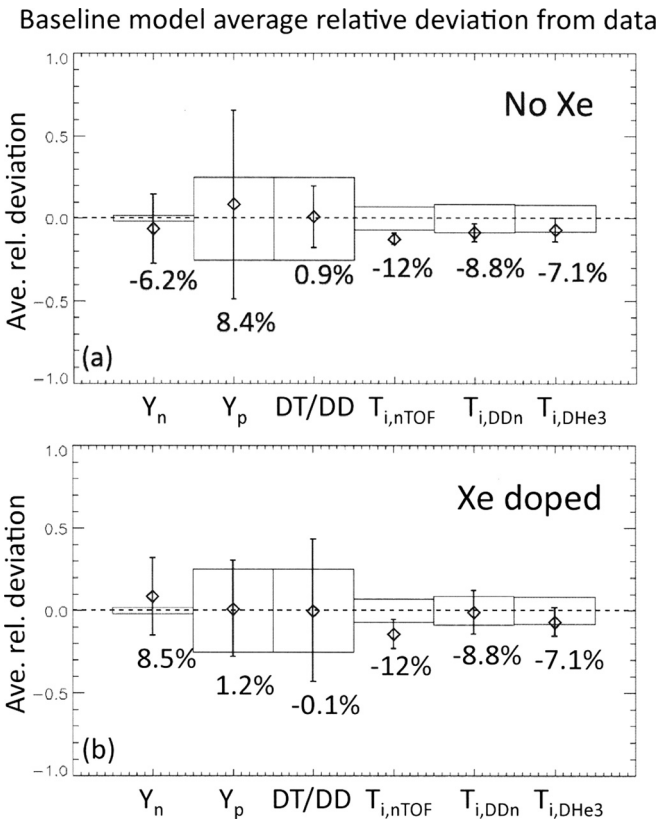

FIG. 1. Average relative deviation of the baseline LASNEX model from the data for the full set of (a) 14 undoped capsules and (b) 13 doped capsules with nominal gas fill (2/3 D2 and 1/3 He3 by pressure), nominal capsule diameter ($\sim 900\,\mu$m), and nominal laser drive (18 kJ, 800 ps square pulse). The data included are the DD neutron yield, the DHe_3 proton yield, the ratio of secondary DT neutrons to primary DD neutrons (the DT/DD ratio), the burn-averaged ion temperature from nTOF, and the DDn- and DHe3-burn-averaged temperatures from the Frenje *et al.* method. Only 9 of these shots have Ti_{DD} and Ti_{DHe3} measurements: 4 with Xe dopant and 5 without. Each result is plotted with a diamond symbol and provided numerically as a percentage (i.e., the undoped neutron yields are 6.2% low on average). Boxes indicate individual experiment measurement uncertainty. Overall, the baseline LASNEX model with DCA NLTE atomic physics gives good agreement with the data.

Reaction-weighted ion temperatures are calculated from the simulations as follows. The instantaneous total reaction rate ($\dot{Y}_{12}$ in units of number/time) for two reactants labeled 1 and 2 is determined by summing over computational zones the product of zonal reaction weight R_{12} (in units of number/volume/time) and cell volume V

$$\dot{Y}_{12} = \sum_{zones} R_{12} V. \tag{1}$$

This total rate is used to create an instantaneous reaction-weighted ion temperature

$$\langle T_i \rangle_{12} = \frac{1}{\dot{Y}_{12}} \sum_{zones} T_i R_{12} V, \tag{2}$$

where T_i is the zonal ion temperature, which is in turn integrated in time to form a burn-averaged ion temperature for the given reaction

$$T_{i,12} = \frac{1}{Y_{12}} \int^t \langle T_i \rangle_{12} \dot{Y}_{12} dt'. \tag{3}$$

The asymptotic (in time) value of Eq. (3) is compared to the DDn and DHe^3 burn averaged temperature inferred from the data via the PPM method described by Frenje *et al.*[16] Note, however, that this data analysis was performed for only 5 of the undoped capsules and 4 of the doped capsules, or about 1/3 of the capsules otherwise represented in Fig. 1.

For both undoped and doped capsules, the yields and DT/DD ratios agree with the data exceptionally well—to better than 10% on average. The DT/DD ratios, which provide a measure of fuel ρR, are on average off by less than 1%.

Burn-weighted ion temperatures determined from nTOF are on average 12% low for undoped capsules, and 14% low for doped capsules. For a characteristic temperature of 7 keV, this corresponds to about 0.8–1 keV, compared to a measurement uncertainty of about 0.5 keV. The uniformity in agreement between doped and undoped capsules indicates that this is not a problem with NLTE modeling of the Xe dopant.

Neutron and proton burn-weighted temperatures determined by the PPM method show somewhat better agreement for the undoped capsules, and agree with the doped capsule data.

B. Dependence on laser intensity

In Fig. 2, we show the individual level of agreement for the undoped capsules, as a function of the laser intensity. We include here the results from series 2 (the larger capsules) in

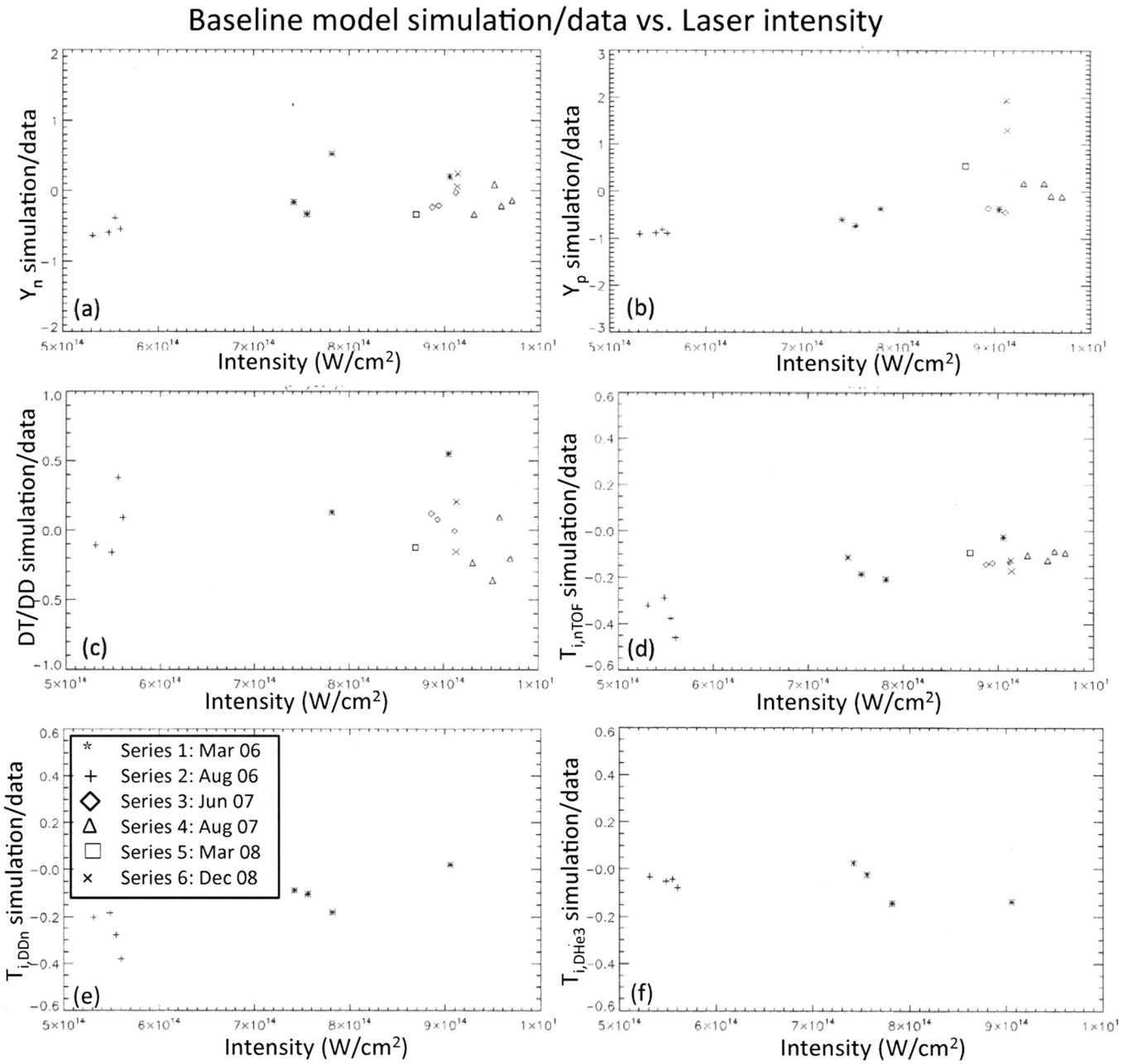

FIG. 2. Relative deviation of the baseline model from the data for individual capsules as a function of laser intensity: (a) DD neutron yield in units of 10^{11}, (b) DHe3 proton yield in units of 10^{10}, (c) DT/DD ratio, (d) nTOF T_i, (e) DDn-weighted T_i, and (f) DHe3-weighted T_i. Each shot series is denoted with a different symbol as shown. The larger-diameter capsules fielded in series 2 are included to extend the range of intensities represented.

order to broaden the range of intensities represented. There is no obvious trend in the level of agreement vs. intensity, as might be expected if laser-plasma interactions were resulting in lower coupling efficiency of the drive energy at the higher intensities. If anything, the proton yield and neutron-weighted temperatures (but not the DHe^3-weighted temperature) suggest a slight trend towards higher values of calculation vs. experiment at higher intensities. This increase is due primarily to an apparent reduced coupling efficiency for the larger diameter series 2 targets, which were driven by the longer duration laser pulse.

C. Effect of Xe dopant

Data and simulation results are plotted together in absolute terms as a function of Xe dopant pressure in Fig. 3, for the full set of nominal capsules with nominal $D:He^3$ ratio. Data are shown in red, binned by Xe dopant pressure, while the black symbols denote simulation results with the baseline model. Because there are small differences in the partial fill pressures of even nominal fill capsules, we use the standard scaling of reaction rate $\propto n_1 n_2$, where n_i are the reacting species, to normalize all absolute yields. In terms of the He^3

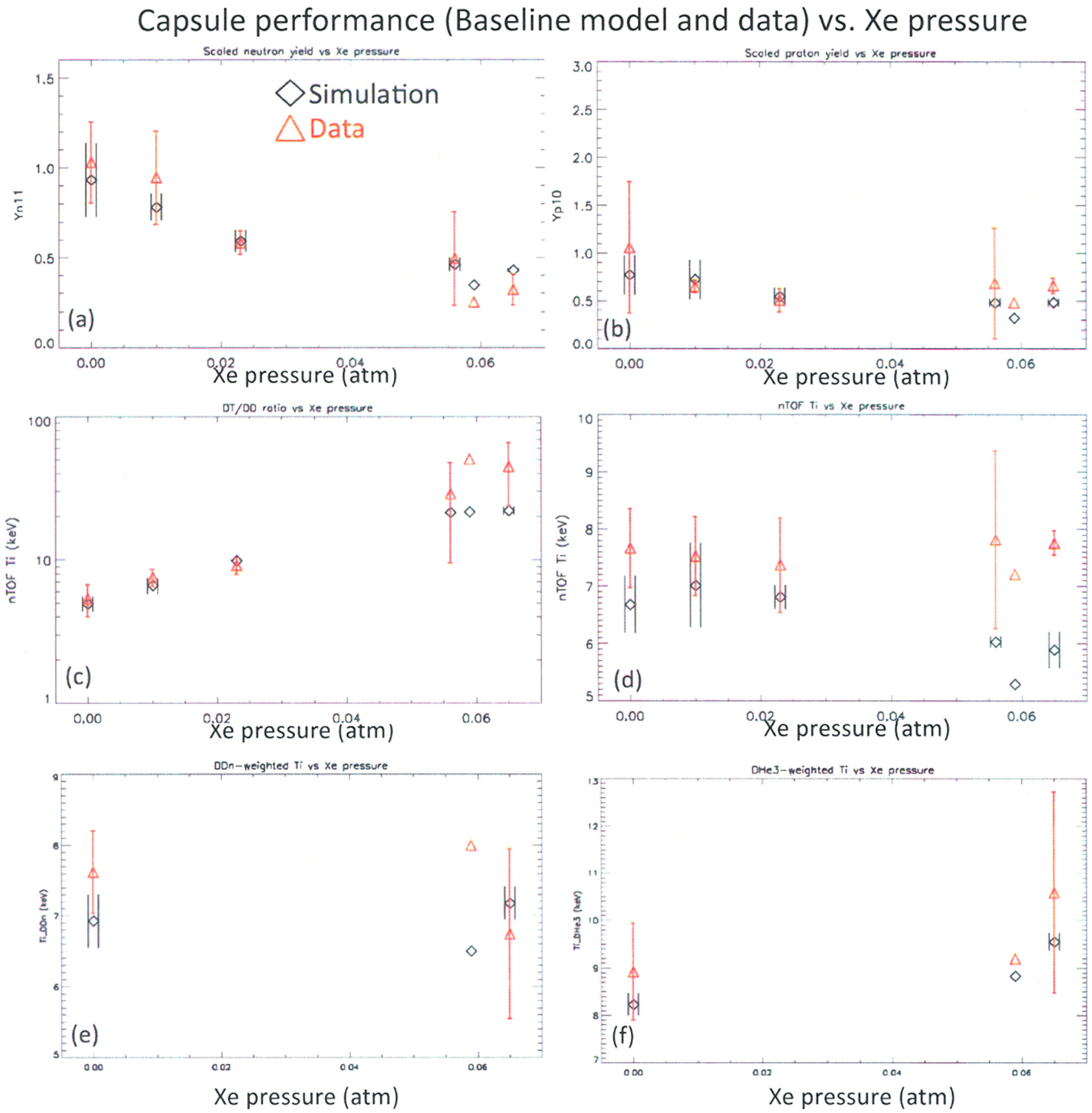

FIG. 3. Simulated and observed capsule performance as a function of Xe dopant pressure, binned by Xe dopant pressure. Error bars denote the standard deviation about the average for targets with a given Xe dopant pressure. Single centered error bars correspond to data, while double offset error bars correspond to simulation results. Data is shown in red, and simulation results are shown in black. The baseline LASNEX model with DCA is in agreement with many details of capsule performance over a range of Xe concentrations.

fraction and fill pressures, and assuming constant convergence ratio, we have

$$Y_{DD} \propto P_D^2 = 4P_D^2 = 4\frac{(1-f_{He3})^2}{(1+f_{He3})^2}P_{tot}^2, \tag{4a}$$

$$Y_{DHe3} \propto P_D P_{He3} = 4\frac{f_{He3}(1-f_{He3})}{(1+f_{He3})^2}P_{tot}^2. \tag{4b}$$

With the nominal fill parameters of $f_{He3}=0.2$, $P_{tot}=10$ atm, gives

$$\tilde{Y}_{DD} \equiv Y_{DD}\left[\frac{3}{2}\frac{(1-f_{He3})}{(1+f_{He3})}\frac{P_{tot}}{10\,\text{atm}}\right]^{-2}, \tag{5a}$$

$$\tilde{Y}_{DHe3} \equiv Y_{DHe3}\left[\frac{3\sqrt{f_{He3}(1-f_{He3})}}{(1+f_{He3})}\frac{P_{tot}}{10\,\text{atm}}\right]^{-2}, \tag{5b}$$

which reduce to the absolute yields under nominal fill conditions. Equation (5a) is a generalized form of the "hydro-equivalent" scaling used in Ref. 27, in which case $P_{tot}=(4P_{eq}-P_{D2})$, where P_{eq} is the hydrodynamicaly equivalent pure deuterium fill pressure.

Figure 3(a) shows that the scaled DD neutron yield decreases by several times over this range of Xe pressures. Despite its greater temperature sensitivity, the DHe^3 proton yield shows weaker sensitivity to Xe pressure. In both cases, the NLTE simulations accurately capture the effect of the dopant.

The most obvious impact of Xe dopant on capsule performance is observed in the DT/DD neuron ratio (see Fig. 3(c)), which increases an order of magnitude at the higher concentrations, relative to the undoped capsules. In the simulations, this results from enhanced radiative cooling in doped capsules, which increases the compressibility of the capsule and facilitates a collapse to higher convergence ratio. This is correlated with a factor of ~2 decrease in the size of the hot x-ray emitting region, as observed by gated x-ray imager, when Xe is present at the higher concentrations (see Fig. 4).

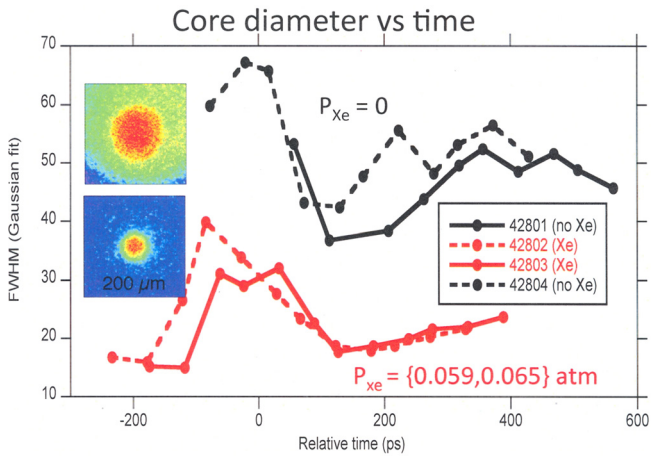

FIG. 4. X-ray imaging data and analysis showing enhanced compression with Xe dopant. The addition of ~0.6% Xe by number gives a factor of ~2 reduction in the x-ray emission core diameter.

The burn-weighted nTOF ion temperatures (Fig. 3(d)) suggest only a weak decrease in burn-weighted ion temperature (no more than ~1 keV) with increasing Xe dopant pressure. The DD neutron- and DHe^3 proton-weighted burn temperatures (all from series 4, see Figs. 3(e) and 3(f)) are insufficient to establish any trends. In the simulations, the DHe^3-weighted ion temperatures actually increase slightly with increasing Xe pressure. This counterintuitive result is explained by the fact that, neglecting radiative losses, a strong shock wave moving through an ideal gas at fixed velocity gives an ion temperature proportional to A, the atomic number of the gas. In our case, where the gas density is low compared to the shell density, the initial shock velocity is set by the deposited laser energy, with only weak dependence on the gas density. Higher-Z dopant gives faster cooling of the plasma, but at these dopant levels the radiative cooling rate is still slow compared to the rate of shock heating. Thus, small amounts of Xe dopant give higher initial ion temperatures than does undoped gas. Since the DHe^3 reaction is more sensitive to temperature than is the DD reaction in this temperature range,[26] it is more strongly weighted towards the early-time shock phase of the implosion. Consequently, the DHe^3 yield reflects more strongly the higher early-time temperature resulting from shock heating of the doped gas.

Thus, the principle effect of a small dopant level is not to decrease the peak ion temperature, but rather to increase the subsequent cooling rate and decrease the time over which high temperatures are maintained. This shortening of the burn width causes a decrease in yield with increasing dopant fraction even when the burn-weighted temperature does not decrease.

The peak electron temperature, as measured by the conical crystal spectrometer, does show a clear decrease even at the lowest Xe dopant concentrations. With $P_{Xe}=0.01$ atm, the peak electron temperature is about 20% lower than in an otherwise similar undoped experiment. Simulations give peak electron temperatures that are ~30% lower than those inferred from measured continuum spectra (~2.6 keV compared to ~3.8 keV for an undoped capsule from shot series 4), but show the same relative change when 0.1 atm Xe is added. Better detector calibrations are needed before making more detailed comparisons of simulated absolute electron temperatures.

D. Dependence on the He3 fraction

Within series 5 and 6, the He3 atomic fill fraction is varied from 0.1 up to 0.85. The measured and simulated DD and DHe^3 yields are plotted in Figs. 5(a) and 5(b). Within each series, the measured yields are unscaled, while the simulated yields shown are normalized to agree on average with the data in that series. The solid lines denote the expected yield scalings from Eq. (4a), neglecting variations in the total fill pressure. Within these two series, the total fill pressure $P_{tot}=10.88\pm0.24$ atm, so the constant pressure approximation is a reasonable one.

In Figs. 5(c) and 5(d), the same yield data is shown normalized to the expected scaling Eq. (4b). Thus, a horizontal

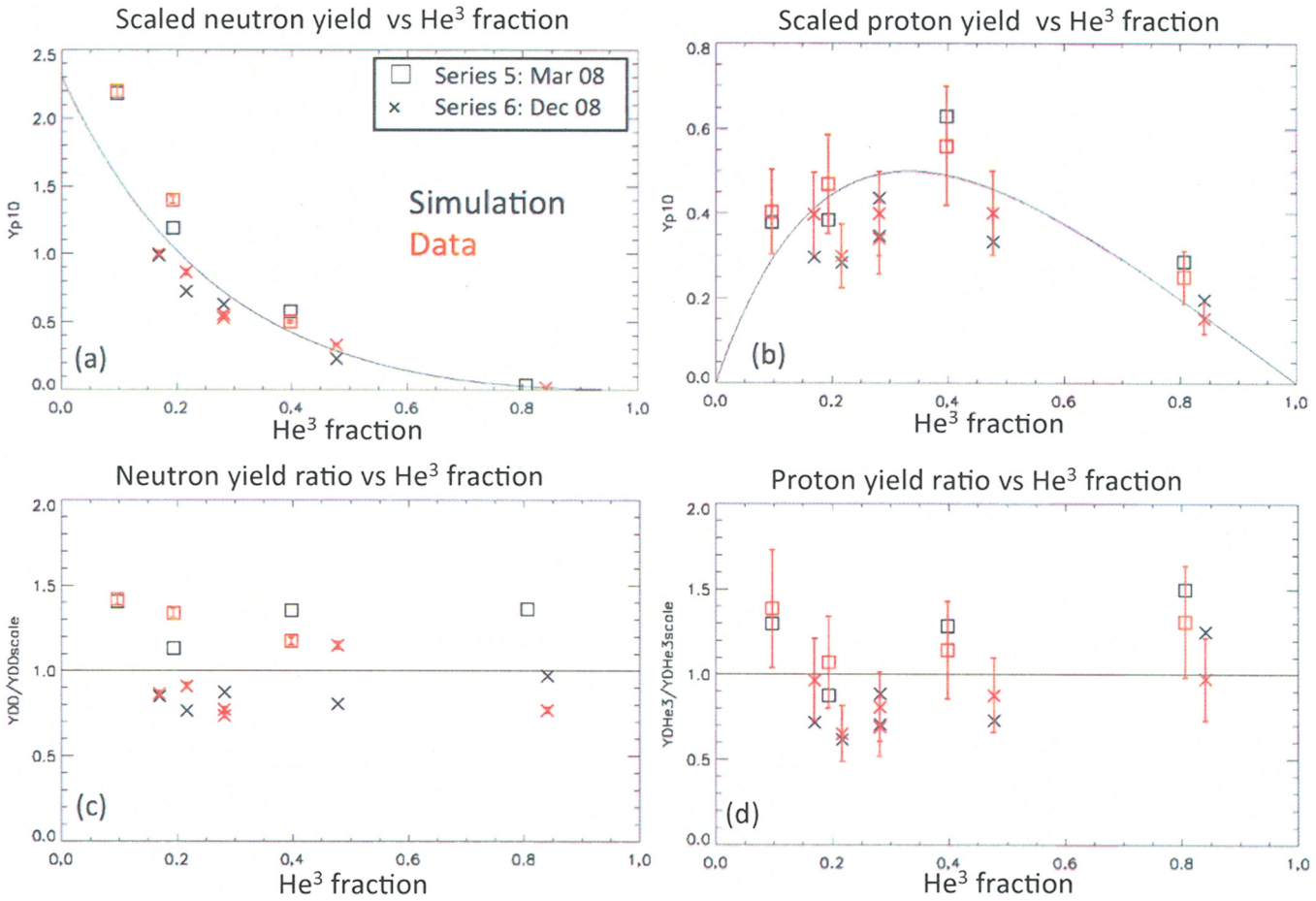

FIG. 5. Dependence of capsule (a) DDn yield and (b) DHe^3 yield on He^3 fill fraction from shot series 5 (square symbols) and shot series 6 (x symbols). Data is shown in red, and simulation results are shown in black. A constant normalization factor is applied to the simulated yields from each shot series to scale out their average deviation from the data. Solid lines denote the scaling expected at constant ion temperature and plasma compression, based solely on initial partial pressures under the approximation of constant total pressure. The ratio of the data to the scaling curve is shown in (c) for DDn yields and (d) for DHe^3 yields. The data are consistent with the expected scaling and most deviations in form are captured by the simulations, indicating no yield anomaly.

line would indicate that the data follow the expected scaling. For both neutron and proton yields, the data and simulations agree well with the theoretical functional form. Furthermore, the deviations from the expected scaling are in large part captured by the numerical simulations, indicating that they result from known variations in capsule dimensions, fill pressure, and laser drive, as well as the resulting calculated variations in plasma temperature, convergence ratio, etc.

In other words, we see nothing of the yield anomaly first reported[27] in DHe^3-filled CH shell implosions. Relative to yields of capsules with either pure D_2 fills or nearly pure He^3 fills, they found DD and DHe^3 yields in equimolar fill capsules that were only about half what they expected based on a yield scaling to which ours is equivalent. The anomaly was reported for capsules ranging in shell thickness from 15 μm to 27 μm, with fill pressures hydrodynamically equivalent to 3 atm and 15 atm pure D_2 fills, and in DHe^3 shock yields as well as DD and DHe^3 compression yields (although the only shock phase results they include are from 20 μm and 24 μm capsules, and the yield anomaly does not appear to be represented by the thinner of the two). By comparison, our capsule diameter is the same as theirs, our nominal-fill hydro equivalent pressure is ~9 atm, our convergence ratio (~15) is about the same as their higher-pressure case, and our ρR (~10 mg/cm^2) and ion temperature (~7 keV) are comparable to their shock-phase values.

The principle difference is that our thinner-shell capsule implosions do not display a distinct, delayed compression phase at lower temperature relative to the shock phase. In our case, the compression phase follows so closely behind the first shock that there is no substantial cooling between the two. Consequently, DHe^3 as well as DD yields are dominated by the short compression phase, which is comprised of a single second shock. Thus, our results might not be inconsistent with other studies with thin glass shells that reported observing a yield and compressibility anomaly for a cooler compression phase yields but not the shock phase.[28] In this study, the compression phase was delayed by employing a shorter (600 ps) laser drive pulse. If, for example, the compressibility of the gas behind the first shock is altered by some means, the effect might not be manifest in our experiments until after the compression phase is already at its end. This would not, however, explain the compression-phase yield anomaly reported by Wilson *et al.*,[24] for capsules nominally identical to ours and driven by the full 1 ns, 23 kJ laser pulse.

VII. ANALYSIS OF SIMULATION RESULTS

A. Effect of mix

One of the goals of this line of experiments is to develop a platform for validating models of electron-ion coupling in nonequilibrium thermonuclear plasmas with and without the presence of a known distribution of atomically-mixed high-Z dopant. Measurement of electron-ion coupling in capsule implosions is complicated, however, when hydrodynamic instabilities inject additional plasma species from the capsule shell into the fuel. Unlike the pre-loaded Xe dopant, this mixed-in shell material has a distribution that depends on both space and time, and is very difficult to measure.

We attempt to capture these processes through application of mix models, which typically include adjustable parameters. Some of these parameters are constrained by dedicated experiments (in shock tubes, for example), while others are adjusted to match capsule yields and other observables. Due to the integrated nature of these implosion experiments, it is possible that deficiencies in an electron-ion coupling model, for example, could be "covered up" by adding more or less mix. In other words, for a system that is susceptible to fuel-shell instabilities, it might be very difficult or even impossible to disentangle plasma coupling effects from mix effects.

Due to their moderate *CR* of ~15, we expect these thin-shell capsules to be less affected by mix than thicker-shell higher-convergence capsules. Nevertheless, we still calculate significant yield reduction due to mix. This is shown in Figs. 6(a) and 6(b), where we plot the simulated yield over clean (YOC) as a function of Xe dopant pressure, for both DD and DHe^3 reactions. The YOC is in this case defined as the ratio of yield from a simulation with the mix model turned on, to the yield when the mix model is turned off.

For DD reactions, we find an average $YOC_n = 0.67$ for undoped capsules, and an average $YOC_n = 0.73$ for Xe-doped capsules. The combined average for doped and undoped capsules is $YOC_n = 0.70$. The increase in YOC with dopant level can be understood as follows: Dopant acts like dynamic mix in the sense that it provides more rapid cooling that reduces the late-time yield. Once the TN reactions have been cut off by dopant-enhanced radiative cooling, there is less room for dynamic mix to have an impact, so even the same amount of dynamic mix will have a lesser relative effect on capsule performance.

The YOC for DHe^3 reactions follows a similar trend, but the values are somewhat higher ($YOC_p = 0.82$ for undoped capsules, 0.85 for doped capsules, and combined average $YOC_p = 0.84$). This reaction is less affected by mix than is the DD reaction due to its stronger temperature

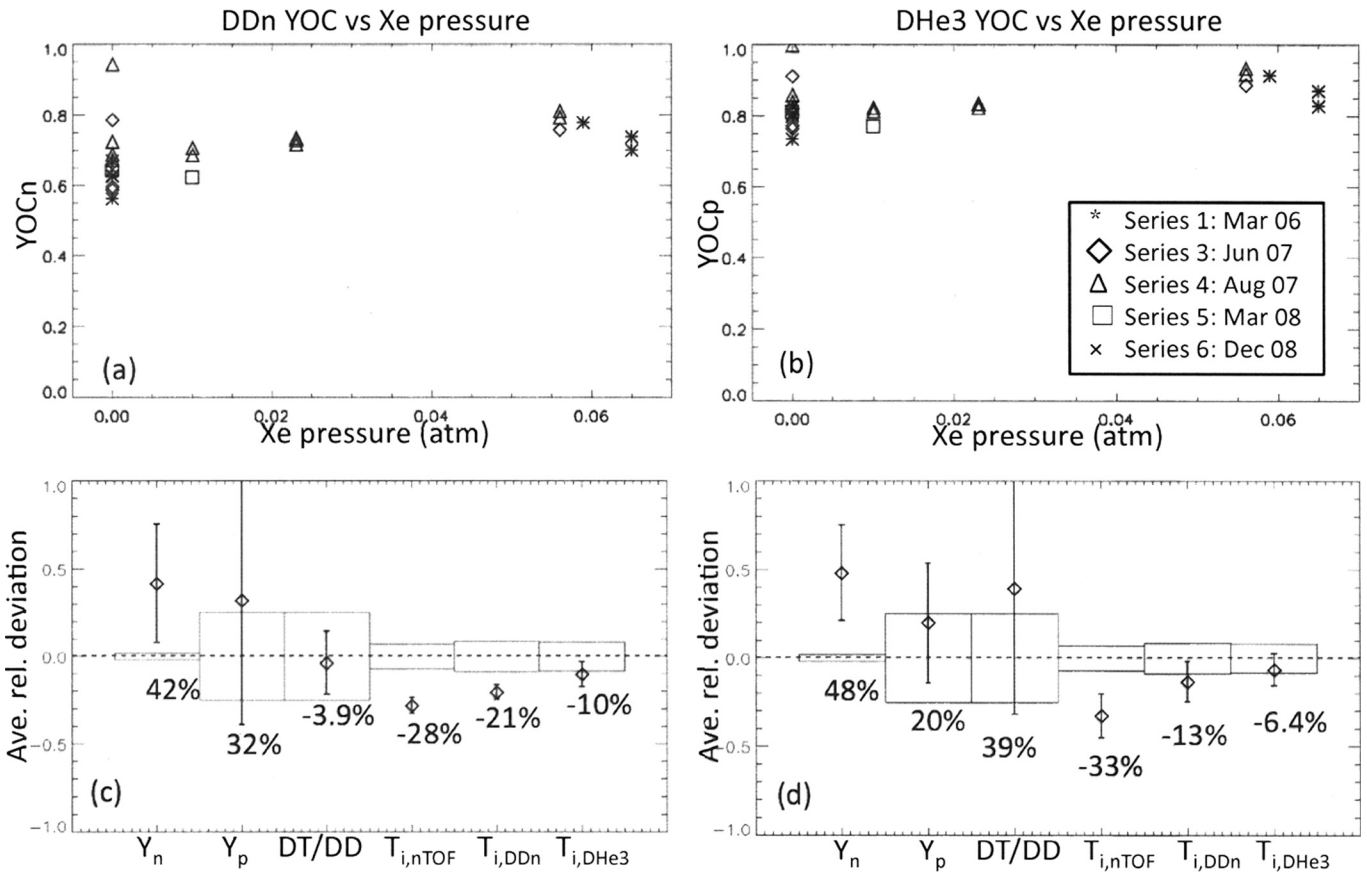

FIG. 6. Effect of hydrodynamic mix on capsule performance as described by the code's mix model. (a) DDn yield over clean (YOC_n) as a function of Xe dopant pressure. (b) DHe3 YOC_p as a function of Xe dopant pressure. Average relative deviation from the data for no-mix "clean" calculations of (c) undoped capsules and (d) Xe-doped capsules. Hydrodynamic mix decreases the thermonuclear yields and increases the burn-weighted ion temperature.

sensitivity (see Fig. 5(c)). Stronger temperature sensitivity means that proportionally more yield comes from the early higher-temperature lower-density first shock phase. This first shock phase occurs before the onset of deceleration-phase Rayleigh-Taylor instabilities.

To get a sense of the uncertainties associated with the level of mix-induced yield degradation, we note that choosing a different value for the laser energy multiplier *lasfac* leads to a different mix treatment to get the best fit to the data set. In the limiting case that $lasfac = 1.0$, we find for undoped capsules an average DDn $YOC_n = 0.55$, and DHe^3 proton $YOC_p = 0.70$. Thus, with higher laser energy absorption efficiency, we need more mix to bring the yields down by an additional 12% to get into the range of the data. The average relative deviation from the neutron and proton yield data is then $13 \pm 33\%$ and $28 \pm 37\%$, respectively. This is still on the high side of acceptable, but it turns out that it is difficult to degrade the yields any further with the mix model unless unreasonable parameter settings are employed. For the doped capsules, the same model gives an average DDn $YOC_n = 0.76$, and DHe^3 proton $YOC_p = 0.85$, but these doped capsule yields are still higher than the data by on average $80 \pm 60\%$ and $78 \pm 46\%$, respectively.

In Figs. 6(c) and 6(d), we show the average relative deviation from the data for clean simulations (i.e., mix model turned off) of undoped (Fig. 6(c)) and doped (Fig. 6(d)) capsules. These can be compared to Fig. 1 to see the calculated effect of mix on the observables. The main point of note is that, in addition to decreasing the yields, mix acts to *increase* the burn-weighted temperatures. This result, which might seem counterintuitive, results from the fact that even without mix the temperature is decreasing in time as the capsule moves into the compression phase and approaches minimum radius. If mix acted to slightly increase the cooling rate while allowing reactions to continue at an appreciable rate, then the result could be a lower burn temperature. But if instabilities rapidly inject mix throughout the fuel shortly after the onset of the deceleration phase, thereby drastically reducing the reaction rates, then the burn-weighted temperatures will be more heavily weighted towards the earlier-time, higher-temperature shock phase. Consequently, such mix will increase the burn-weighted temperatures. It should then be no surprise that the DHe^3-weighted temperature is less impacted by mix than is the neutron-weighted temperature, because the former reaction is already more weighted towards the shock phase due to its stronger temperature sensitivity.

B. Sensitivity to CO_2 concentration

The capsule fabrication process results in 0.1–0.5 atm of gas residual, which is dominated by a CO_2 component. Since the precise residual pressure and composition is not known on a per capsule basis, we have chosen to represent it with a fixed CO_2 pressure of 0.5 atm. The effect of reducing this value down to 0.1 atm in the baseline model, without changing anything else, is shown in Table I.

The effect of residual gas pressure on ion temperatures is no more than 10% for doped as well as undoped capsules.

TABLE I. Average relative deviation from the data for simulations with residual CO_2 pressure of 0.1 atm, compared to the baseline simulation value of $P_{CO2} = 0.5$ atm.

	DDn		DHe^3		DT/DD		nTOF T_i		DDn T_i		DHe^3 T_i	
	No Xe	Xe	No Xe	Xe	No Xe	Xe	No Xe	Xe	No Xe	Xe	No Xe	Xe
0.5 atm	−6	9	8	1	1	0	−12	−14	−9	−1	−7	−7
0.1 atm	31	80	39	70	33	24	−9	−5	−12	6	−17	−7
Δ%	+37	+71	+31	+69	+32	+24	+3	+9	−3	+7	−10	+0

For undoped capsules, moving to the low end of the residual pressure range increases yields and DT/DD ratio by 30%–40%. In Xe doped capsules, the DT/DD ratio is somewhat less sensitive than in undoped capsules, but the yields increase by about 70%. In this case, we would require mix to provide lower YOC to make up the difference. Since mix tends to reduce doped capsule yields less than undoped yields, it would be difficult to use mix alone to reconcile the simulations with P_{CO2} to all the data. Indeed, this is why we settled on the upper end of given range for the simulation baseline.

C. Sensitivity to atomic physics model

The data from doped capsule implosions give a clear illustration of the dynamically significant NLTE nature of these implosions, and provide a means of comparing NLTE models within the hydro code. As was detailed earlier, the baseline model uses the DCA atomic physics package to model high-Z doped gas. Results with the simpler XSNQ NLTE model are shown in Fig. 7.

Whereas the simulations with DCA on average gave very good agreement with the observed yields and fuel compression (via the DT/DD neutron ratio), XSNQ overcalculates the yields by 70%–80% on average, and undercalculates the compression by about 50% on average. The same is shown in Figs. 7(b)–7(d) as a function of Xe dopant pressure. In contrast to the data, there is almost no increase in the simulated DT/DD ratio with increasing dopant level, indicating very little radiative cooling enhancement and consequent collapse to higher fuel compression.

The nTOF burn-weighted ion temperature is on average ~0.8 keV higher than with DCA, which places it in agreement with the data. However, temperatures of capsules without Xe dopant remain significantly lower than the data when run with XSNQ, similar to the results with DCA or LTE. Correcting whatever is responsible for these systematically low temperatures in undoped capsules would likely give a similar increase in the doped capsule XSNQ calculations, resulting in overly high temperatures in that case.

While XSNQ significantly underpredicts the enhancement in radiative cooling due to the high-Z dopant, LTE does just the opposite (see Fig. 8). Neutron and proton yields are low on average by 17% and 34%, respectively. The deviation in simulated neutron yields is not uniform across the range of Xe dopant levels. At the highest level, in fact, they agree well with the data (somewhat better than DCA does),

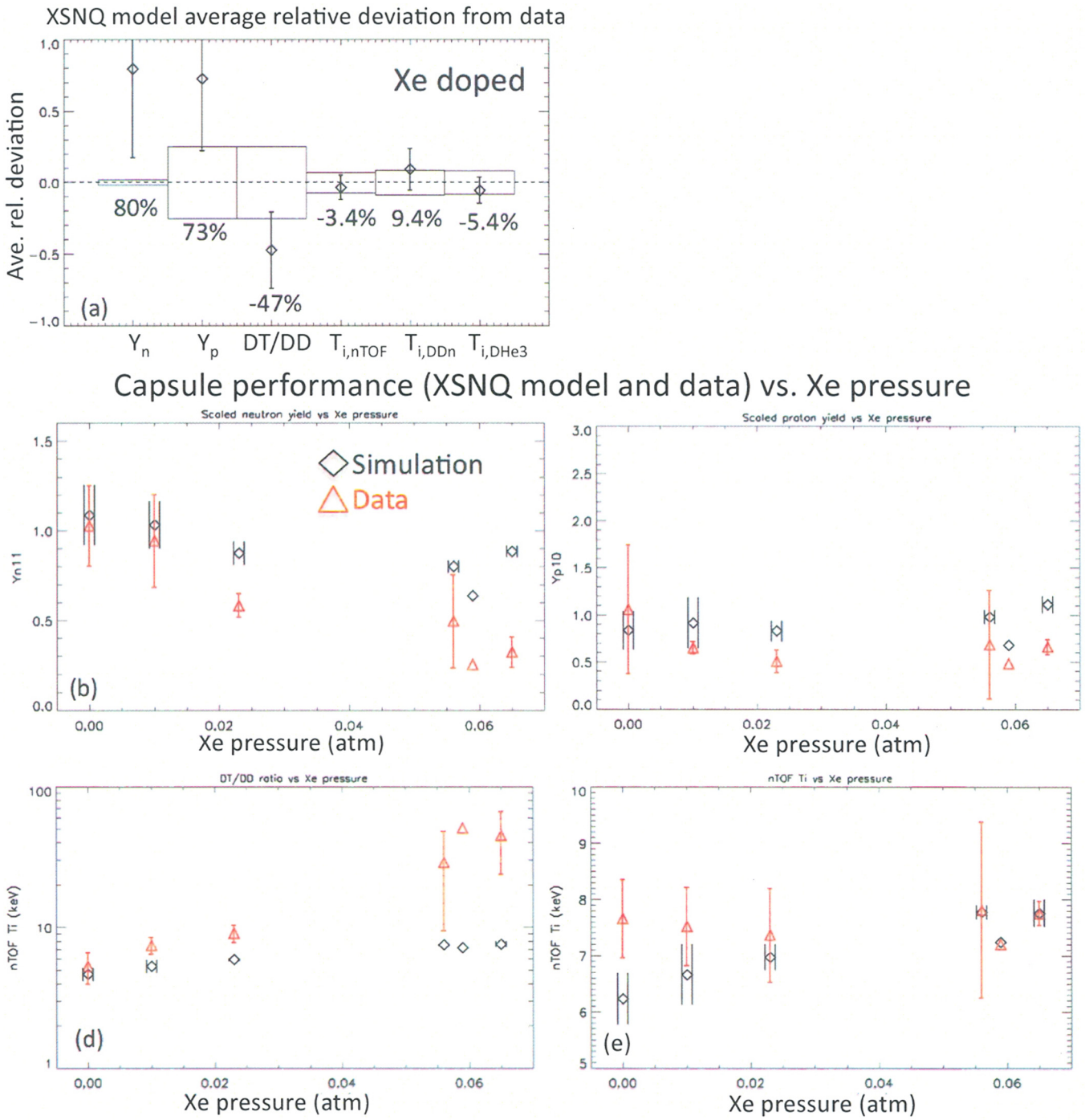

FIG. 7. Simulated capsule performance with XSNQ NLTE atomic physics model. (a) Average relative deviation of the simulations from the data. Dependence on Xe dopant pressure for (b) scaled DDn yield, (c) scaled DHe3 yield, (d) DT/DD ratio, and (e) nTOF ion temperature, binned by Xe dopant pressure. XSNQ significantly underpredicts the enhancement in radiative cooling due to the high-Z dopant.

which might indicate that the most heavily doped systems are approaching LTE as they collapse towards capsule minimum volume. Proton yield rates fall off faster as the plasma moves into the denser but cooler compression phase, which would explain why the same trend is not apparent in the DHe^3 yields. On average, DT/DD ratios are high by nearly 200%, and nTOF temperatures are low by more than 40%. All of the above is consistent with a significant overprediction of the radiative cooling enhancement and collapse due to the high-Z dopant.

D. Sensitivity to electron ion coupling

Within the numerical simulations, a constant multiplier *eicplm* can be applied to the electron-ion coupling coefficient, allowing us to investigate sensitivities of the observables. Both undoped and doped capsules performance shows significant sensitivity to the coupling multiplier when it is varied over a range of 0.5–2.0 (see Fig. 9). Simulated observables are on average consistent with the data over the ranges of *eicplm* shown in Table II. Results are given separately for

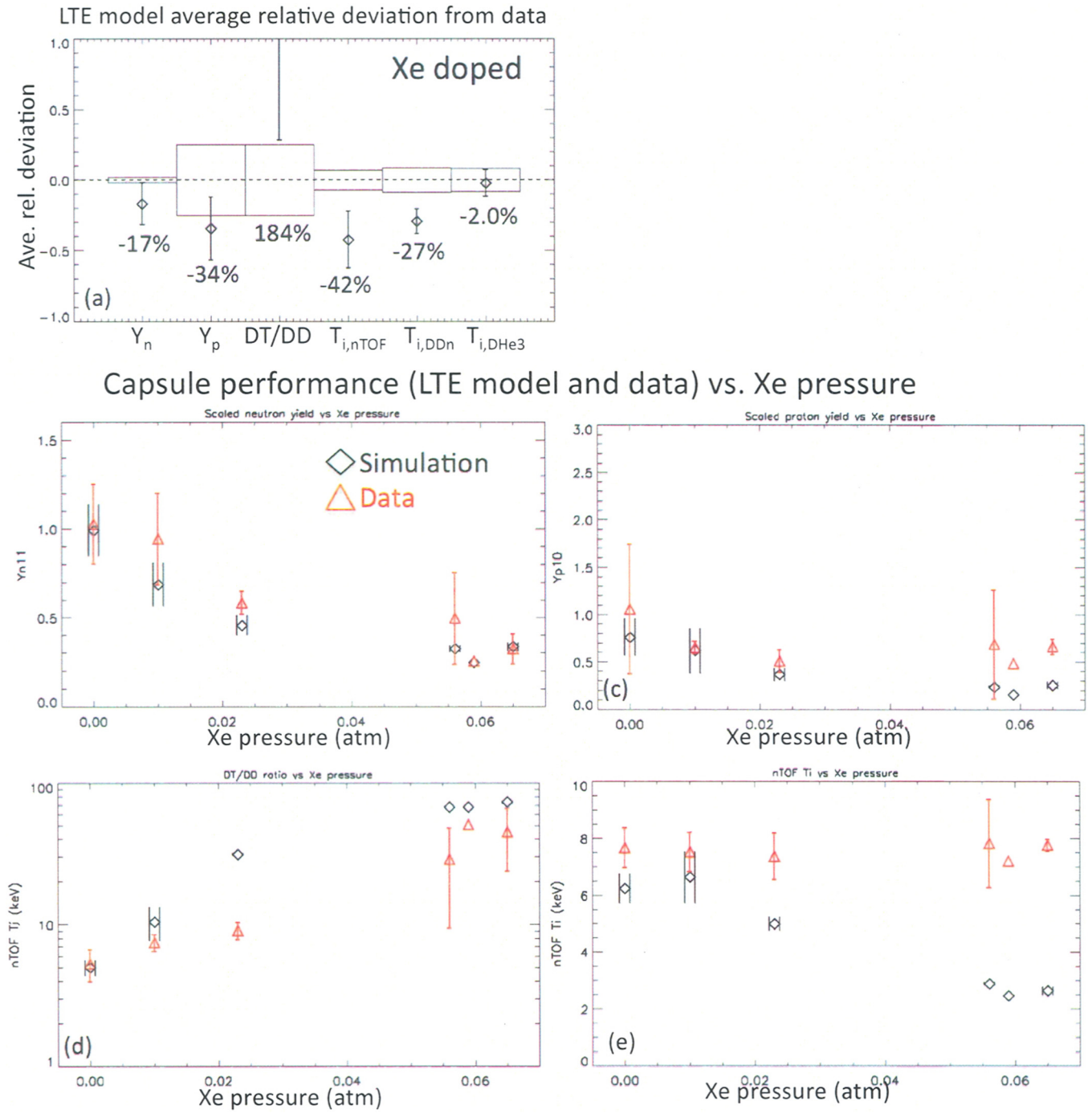

FIG. 8. Simulated capsule performance with LTE equations of state and opacities in the fuel. (a) Average relative deviation of the simulations from the data. Dependence on Xe dopant pressure for (b) scaled DDn yield, (c) scaled DHe3 yield, (d) DT/DD ratio, (e) and nTOF ion temperature, binned by Xe dopant pressure. LTE significantly overpredicts the enhancement in radiative cooling due to the high-Z dopant.

undoped and doped capsules in order to provide a clean plasma result independent of uncertainties in NLTE physics modeling. That said, it turns out that the inferred electron-ion coupling multiplier is largely consistent across the full data set. Simulated yields and DT/DD ratio are consistent with the data over a fairly narrow range of $eicplm = 0.9$–1.2, which is relatively close to unity. This range is constrained at both ends by the yield data, as the DT/DD ratios are consistent with the full range of *eicplm* considered. Incorporating in the nTOF ion temperature data, which we have already noted is systematically higher than the baseline simulation model, we find $eicplm = 0.8$ for undoped capsules and $eicplm = 0.9$ for doped capsules.

As noted earlier, uncertainties in the hydrodynamic mix make it more difficult to use these data to infer the electron-ion coupling strength. But in this case it does not preclude it either. For $eicplm > 1$, the simulated yields and temperatures are higher than the data. We could increase the mix to bring down the yields (increase the YOC), but as we have discussed above and shown in Fig. 6, this tends to further increase the burn-weighted temperature, which would move it further away from the data. Similarly, $eicplm < 1$ gives

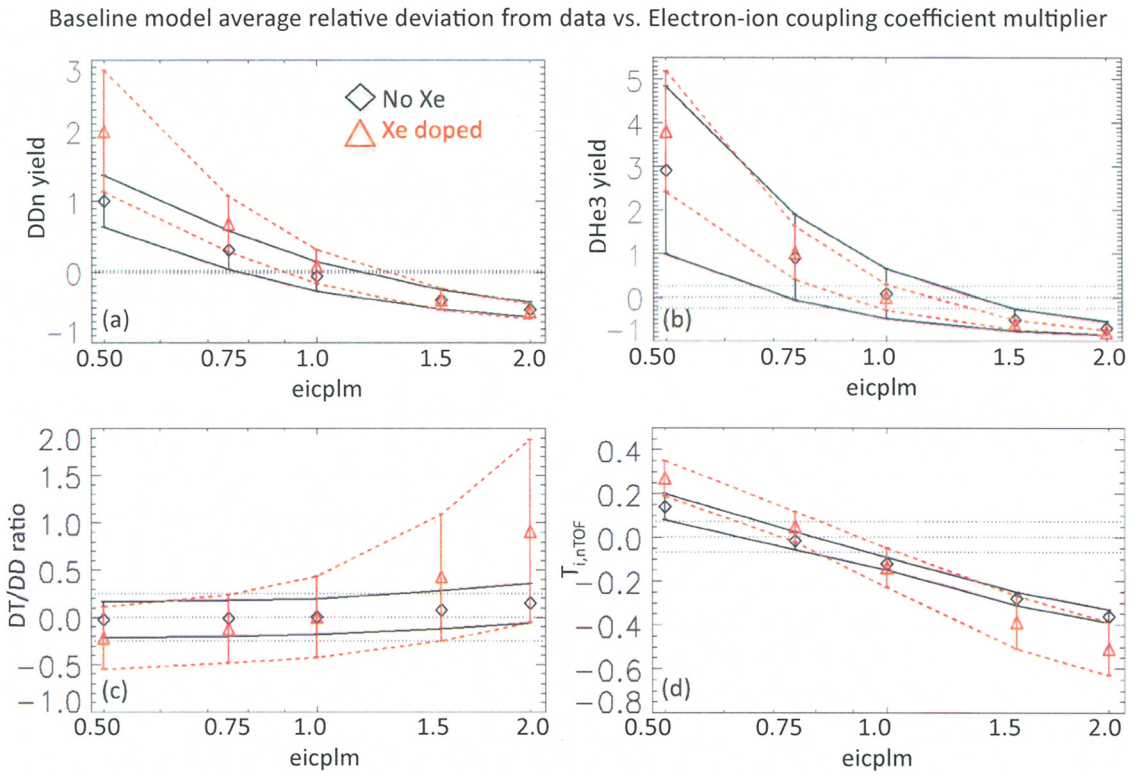

FIG. 9. Effect of ion-electron coupling coefficient multiplier (*eicplm*) on the agreement between the baseline LASNEX model and the data. Results are shown in black for undoped capsules and red for doped capsules. Error bars denote the standard deviation in the simulation-data comparison across the set of 14 undoped capsules and 13 Xe-doped capsules. Horizontal dotted lines indicate the single shot experimental uncertainty. Thermonuclear (a) neutron and (b) proton yields are consistent with an electron-ion coupling multiplier in the range of 0.9–1.2. (c) The DT/DD ratio is not sufficiently sensitive to electron-ion coupling to constrain the model within the range of *eicplm* = 0.5–2.0. (d) The ion temperature from nTOF, which is systematically low in the baseline model, agrees with the undoped capsule data for *eicplm* ~ 0.8, and the doped capsule data for *eicplm* ~ 0.9.

TABLE II. Range of electron-ion coupling coefficient multiplier values for which the baseline simulation model is consistent with the data set.

	No Xe	Xe-doped
DDn yield	0.8–1.2	0.9–1.3
DHe3 yield	0.7–1.4	0.9–1.2
DT/DD ratio	0.5–2.0	0.5–2.0
nTOF Ti	0.6–0.8	0.7–0.9
Yields and yield ratio	0.8–1.2	0.9–1.2
All data	0.8	0.9

simulated yields and temperatures that are too low. Decreasing the mix would increase the yields but further decrease the burn temperature. Furthermore, with the baseline model's average YOC ~ 0.7–0.8, even clean calculations would disagree with the data for *eicplm* = 0.5.

VIII. CONCLUSIONS

We have fielded thin-shell DHe^3-filled glass capsules on the Omega laser to provide a fast-implosion experimental platform for developing separate time-resolved measurements of ion, electron, and radiation temperatures in nonequilibrium LTE and NLTE plasmas. Dynamically significant NLTE conditions are created by the addition of the high-Z Xe dopant to the DHe^3 gas fill, in quantities sufficient to have a significant impact on yields, compression, and cooling rates.

A baseline LASNEX simulation model has been developed that shows very good agreement with the data for Xe-doped as well as undoped capsules. Only the burn-weighted ion temperatures show a significant systematic deviation from the data (about 15% low on average). The uniformity of the temperature deviation across dopant levels, together with the degree to which other observables are reproduced, suggest that the discrepancy is not related to deficiencies in NLTE atomic physics modeling.

The baseline model captures the behavior of the capsule when the D:He^3 ratio is varied well away from equimolar, suggesting no yield anomaly with nearly pure deuterium or He^3 fills.

The main effect of the high-Z dopant is to increase the radiative cooling rate in the plasma, allowing it to collapse in compressions that can be an order of magnitude higher than in undoped capsules. At low dopant concentrations, this is done without a significant decrease in the peak or burn-weighted plasma ion temperatures, but thermonuclear yields are still reduced because the faster radiative cooling limits the time over which high temperatures are sustained. The DCA NLTE model agrees well with yield and compression data across the range of Xe dopant levels, and gives a neutron-weighted temperature that is less than 15% lower on average than the data. LTE models dramatically overpredict

the radiative cooling enhancement. Conversely, the same effect is significantly underpredicted by the XSNQ NLTE model, which gives almost no increase in DT/DD neutron ratio over the Xe dopant range studied.

The agreement between the baseline DCA model and the data is decreased when the electron-ion coupling coefficient multiplier in the code is varied away from unity, suggesting that the model is good to within ~20%. The fact that burn-weighted ion temperatures are systematically low in the simulations might result from an electron-ion coupling coefficient that is ~20% too high. However, reliably inferring electron-ion coupling strength from the data is complicated by uncertainties in the hydrodynamic mix, as well as other "knobs" used in modeling the data set. For example, another possible explanation for the low nTOF temperatures is that hydrodynamic mix is cutting off the yield faster than is predicted by the model.

These uncertainties could be largely mitigated in follow-on experiments with larger capsules and more laser energy, which can be performed at the National Ignition Facility (NIF). These would be true exploding pusher capsules in the sense that the entire shell is ablated during the implosion process, resulting in much lower convergence ratio ($CR \sim 4$ compared to the Omega capsule $CR \sim 15$) and almost no susceptibility to mix.[29] Introduction of a fill tube rather than relying on the current diffusion fill process would allow for removal of gas residuals such as CO_2. Higher electron temperatures should allow for better electron temperature history measurements from Kr line emission in addition to bremmstrahlung continuum, thereby bringing higher fidelity to the plasma coupling characterization. Finally, a reliable calculation or a measurement (as in Dodd *et al.*[23]) of the backscattered laser energy vs. time would break the degeneracy associated with adjusting in concert the laser energy multiplication factor and the electron flux limiter. This capability is now available on OMEGA (Ref. 30) as well as NIF,[31] and could be included in future analyses of our existing data set.

ACKNOWLEDGMENTS

This work was performed under the auspices of the U.S. Department of Energy by Lawrence Livermore National Laboratory in part under Contract W-7405-Eng-48 and in part under Contract DE-AC52-07NA27344.

[1]Ya. B. Zel'dovich and Yu. P. Raizer, *Physics of Shock Waves and High-Temperature Hydrodynamic Phenomena*, edited by W. D. Hayes and R. F. Probstein (Dover Mineola, NY, 2002).
[2]S. Atzeni and J. Meyer-ter-Vehn, *The Physics of Inertial Fusion* (Oxford University Press, New York, 2004).
[3]J. I. Castor, *Radiation Hydrodynamics* (Cambridge University Press, New York, 2004).
[4]T. R. Boehly, D. L. Brown, R. S. Craxton *et al.*, Opt. Commun. **133**, 495 (1997).
[5]A. Nikroo, F. H. Elsner, D. G. Czechowicz, J. Gibson, S. E. Grant, A. L. Greenwood, M. L. Hoppe, D. Hysband, B. W. McQuillan, W. J. Miller, J. M. Ponteandolfo, D. A. Steinman, R. B. Stevens, K. R. Schulkz, and M. Takagi, "Capsule production and development for ICF experiments," General Atomics Report GA-A23228, 1999.
[6]R. A. Lerche, D. W. Phillion, and G. L. Tietbohl, Rev. Sci. Instrum. **66**, 933 (1995).
[7]C. Stoeckl, V. Yu. Glebov, S. Roberts *et al.*, Rev. Sci. Instrum. **74**, 3 (2003).
[8]J. A. Frenje, C. K. Li, F. H. Séguin *et al.*, Phys. Plasmas **11**, 2798 (2004).
[9]R. A. Lerche and T. J. Murphy, Rev. Sci. Instrum. **63**, 4880 (1992).
[10]E. G. Gamalii, S. Yu. Gus'kov, O. N. Krokhin, and V. B. Rozanov, JETP Lett. **21**, 70 (1975).
[11]T. E. Blue and D. B. Harris, Nucl. Sci. Eng. **77**, 463 (1981).
[12]T. E. Blue, J. W. Blue, J. S. Durhan, D. B. Harris, A. S. Hnesh, and J. J. Reyes, J. Appl. Phys. **54**, 615 (1983).
[13]H. Azechi, N. Miyanaga, R. O. Stapf, K. Itoga, H. Nakaishi, M. Yamanaka, H. Shiraga, R. Tsuji, S. Ido, K. Nishihara, Y. Izawa, T. Yamanaka, and C. Yamanaka, Appl. Phys. Lett. **49**, 555 (1986).
[14]M. D. Cable, S. M. Lane, S. G. Glendinning, R. A. Lerche, M. S. Singh, D. H. Munro, S. P. Hatchett, K. G. Estabrook, and L. J. Suter, Bull. Am. Phys. Soc. **31**, 1461 (1986).
[15]F. H. Séguin, J. A. Frenje, C. K. Li *et al.*, Rev. Sci. Instrum. **74**, 975 (2003).
[16]J. Frenje *et al.*, in APS/DPP meeting, Savannah, Georgia, 2004.
[17]T. A. Hall, J. Phys. E **17**, 110 (1984).
[18]J. F. Seely, C. A. Back, C. Constantin, R. W. Lee, H.-K. Chung, L. T. Hudson, C. I. Szabo, A. Henins, G. E. Holland, R. Atkin, and L. Marlin, J. Quant. Spectrosc. Radiat. Transf. **99**, 572 (2006).
[19]J. A. Harte, W. E. Alley, D. S. Bailey, J. L. Eddleman, and G. B. Zimmerman, "LASNEX—A 2-D Physics Code for Modeling ICF," UCRL-LR-105821-96-4 (1996). Copies may be ordered from the National Technical Information Service, Springfield, VA 22161.
[20]C. Malone, R. L. McCrory, and R. L. Morse, Phys. Rev. Lett. **34**, 721 (1975).
[21]W. A. Lokke and W. H. Grasberger, Report No. UCRL-52276 (1977). Copies may be ordered from the National Technical Information Service, Springfield, VA 22161.
[22]H. Scott and S. Hansen, High Energy Density Phys. **6**, 39 (2010).
[23]E. S. Dodd, J. F. Benage, G. A. Kyrala, D. C. Wilson, F. J. Wysocki, W. Seka, V. Yu. Glebov, C. Stoeckl, and J. A. Frenje, Phys. Plasmas **19**, 042703 (2012).
[24]D. C. Wilson, G. A. Kyrala, J. F. Benage, Jr., F. J. Wysocki, M. A. Gunderson, W. J. Garbett, V. Yu, Glebov, J. Frenje, B. Yaakobi, H. W. Herrmann, J. H. Cooley, L. Welser- Sherrill, C. J. Horsfield, and S. A. Roberts, J. Phys.: Conf. Ser. **112**, 022015 (2008).
[25]W. J. Garbett, S. James, G. A. Kyrala, D. C. Wilson, J. F. Benage, F. J. Wysocki, M. A. Gunderson, J. Frenje, R. Petrasso, V. Yu, Glebov, and B. Yaakobi, J. Phys.: Conf. Ser. **112**, 022016 (2008).
[26]H.-S. Bosch and G. M. Hale, Nucl. Fusion **32**, 611 (1992).
[27]J. R. Rygg, J. A. Frenje, C. K. Li, F. H. Seguin, R. D. Petrasso, J. A. Delettrez, V. Yu. Glebov, V. N. Goncharov, D. D. Meyerhofer, S. P. Regan, T. C. Sangster, and C. Stoeckl, Phys. Plasmas **13**, 052702 (2006).
[28]H. W. Herrmann, J. R. Langenbrunner, J. M. Mack, J. H. Cooley, D. C. Wilson, S. C. Evans, T. J. Sedillo, G. A. Kyrala, S. E. Caldwell, C. S. Young, A. Nobile, J. Wermer, S. Paglieri, A. M. McEvoy, Y. Kim, S. H. Batha, C. J. Horsfield, D. Drew, W. Garbett, M. Rubery, V. Yu. Glebov, S. Roberts, and J. A. Frenje, Phys. Plasmas **16**, 056312 (2009).
[29]M. D. Rosen and J. H. Nuckolls, Phys. Fluids **22**, 1393 (1979).
[30]R. K. Kirkwood, T. McCarville, D. H. Froula, B. Young, D. Bower, N. Sewall, C. Niemann, M. Schneider, J. Moody, G. Gregori, F. Holdener, M. Chrisp, B. J. MacGowan, S. H. Glenzer, and D. S. Montgomery, Rev. Sci. Instrum. **75**, 4174 (2004).
[31]D. H. Froula, D. Bower, M. Chrisp, S. Grace, J. H. Kamperschroer, T. M. Kelleher, R. K. Kirkwood, B. MacGowan, T. McCarville, N. Sewall, F. Y. Shimamoto, S. J. Shiromizu, B. Young, and S. H. Glenzer, Rev. Sci. Instrum. **75**, 4168 (2004).